Nanoscale Advances

ROYAL SOCIETY OF CHEMISTRY

PAPER

View Article Online
View Journal | View Issue

Cite this: *Nanoscale Adv.*, 2021, **3**, 3799

Biocompatibility, uptake and subcellular localization of bacterial magnetosomes in mammalian cells†

Frank Mickoleit,[a] Cornelia Jörke,[b] Stefan Geimer,[c] Denis S. Maier,[a] Jörg P. Müller,[d] Johanna Demut,[b] Christine Gräfe,[b] Dirk Schüler *[a] and Joachim H. Clement *[b]

Magnetosomes represent biogenic, magnetic nanoparticles biosynthesized by magnetotactic bacteria. Subtle biological control on each step of biomineralization generates core–shell nanoparticles of high crystallinity, strong magnetization and uniform shape and size. These features make magnetosomes a promising alternative to chemically synthesized nanoparticles for many applications in the biotechnological and biomedical field, such as their usage as biosensors in medical diagnostics, as drug-delivery agents, or as contrast agents for magnetic imaging techniques. Thereby, the particles are directly applied to mammalian cells or even injected into the body. In the present work, we provide a comprehensive characterization of isolated magnetosomes as potential cytotoxic effects and particle uptake have not been well studied so far. Different cell lines including cancer cells and primary cells are incubated with increasing particle amounts, and effects on cell viability are investigated. Obtained data suggest a concentration-dependent biocompatibility of isolated magnetosomes for all tested cell lines. Furthermore, magnetosome accumulation in endolysosomal structures around the nuclei is observed. Proliferation rates are affected in the presence of increasing particle amounts; however, viability is not affected and doubling times can be restored by reducing the magnetosome concentration. In addition, we evidence magnetosome–cell interactions that are strong enough to allow for magnetic cell sorting. Overall, our study not only assesses the biocompatibility of isolated magnetosomes, but also evaluates effects on cell proliferation and the fate of internalized magnetosomes, thereby providing prerequisites for their future *in vivo* application as biomedical agents.

Received 29th December 2020
Accepted 15th May 2021

DOI: 10.1039/d0na01086c

rsc.li/nanoscale-advances

Introduction

Magnetic nanoparticles are of increasing interest for plenty of applications in the fields of cellular biotechnology and biomedicine. The latter include their future usage as *e.g.* biosensors in medical diagnostics, as contrast agents for magnetic imaging techniques, or as agents for controlled drug delivery.[1–5] Depending on the envisioned application, a narrow size distribution in the range from 30–200 nm is required as smaller particles show no sufficient magnetization, whereas larger particles are not able to cross the barrier through the capillaries to reach their targets.[6,7] However, controlling the mean particle size and providing suspensions of high, uniform crystallinity is still challenging.[8,9] A promising alternative to chemically synthesized nanoparticles might be provided by bacterial magnetosomes biosynthesized by magnetotactic bacteria like the alphaproteobacterium *Magnetospirillum gryphiswaldense* (Fig. 1A). Magnetosomes consist of a core of chemically pure magnetite (Fe_3O_4) enveloped by a proteinaceous phospholipid bilayer, the magnetosome membrane, and are therefore reminiscent to magnetic core–shell nanoparticles (Fig. 1B and C).[10,11] The latter harbors a set of magnetosome-

[a]*Dept. Microbiology, University of Bayreuth, D-95447 Bayreuth, Germany. E-mail: dirk.schueler@uni-bayreuth.de*

[b]*Dept. Hematology and Medical Oncology, Jena University Hospital, D-07747 Jena, Germany. E-mail: joachim.clement@med.uni-jena.de*

[c]*Electron Microscopy, University of Bayreuth, D-95447 Bayreuth, Germany*

[d]*Institute of Molecular Cell Biology, Center for Molecular Biomedicine (CMB), Jena University Hospital, D-07745 Jena, Germany*

† Electronic supplementary information (ESI) available: Supplementary methods: fluorescence microscopy. Supplementary figures: Fig. S1, relative fluorescence of DyLight 488 labelled magnetosomes; Fig. S2, hydrodynamic diameters of WT magnetosomes and particle agglomerates; Fig. S3, transmission electron microscopy images of isolated magnetosomes; Fig. S4, fluorescence microscopy analysis of magnetosome internalization by FaDu cells; Fig. S5, transmission electron micrographs of FaDu cells with internalized magnetosomes; Fig. S6, microscopic analysis of FaDu-NR cells incubated with different amounts of isolated magnetosomes, Fig. S7, spheroid formation of FaDu-NR cells after magnetosome-labelling. Supplementary tables: Table S1, bacterial strains and mammalian cell lines used in this study; Table S2, statistical analysis on PrestoBlue cell viability data; Table S3, cell death rates for different mammalian cell lines incubated with isolated magnetosomes; Table S4, statistical analysis on the cell death rates of magnetosome-treated BeWo, FaDu, HCC78, and hPC-PL cells. See DOI: 10.1039/d0na01086c

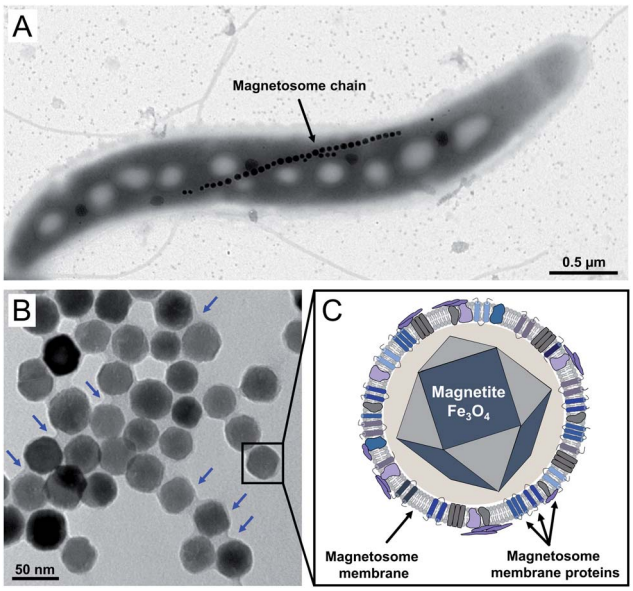

Fig. 1 (A) Transmission electron microscopy (TEM) micrograph of a representative cell of the wildtype strain of *M. gryphiswaldense*. The latter biosynthesizes ~40 magnetosomes per cell arranged in a chain-like manner ad midcell. (B) TEM micrograph of a suspension of isolated magnetosomes (negatively stained) containing well-dispersed particles of ~35 nm in diameter. Magnetosomes consist of a cuboctahedral, monocrystalline core of pure magnetite (Fe_3O_4) that is surrounded by an electron-light organic shell (indicated by blue arrows), representing the magnetosome membrane. (C) Schematic illustration of a single magnetosome nanoparticle. The magnetite core is enveloped by a phospholipid bilayer (magnetosome membrane) that harbours a set of magnetosome specific proteins (Mam proteins).

specific proteins that fulfil functions in particle biosynthesis.[12–14] Strict control on each step of biomineralization enables the generation of particles with a narrow size distribution and uniform morphology, exhibiting characteristics that can hardly be achieved by chemical synthesis (high crystallinity, strong magnetization and stable magnetic moments).[15–18] Due to these features magnetosomes have been envisioned as promising tools for many applications in the biomedical and biotechnological field.[19,20]

Magnetosomes were already successfully tested for cancer treatment using magnetic hyperthermia[21–25] and as contrast agents for magnetic resonance imaging (MRI).[24,26–28] In addition, their internalization by different types of carcinoma cells has been investigated. For instance, Mannucci and co-workers could demonstrate a strong particle uptake by human colon carcinoma HT-29 cells, revealing three phases of interaction (*i.e.* adherence, transport and accumulation in Golgi vesicles).[24] Although the analysis and evaluation of biocompatibility is of great importance for the use of nanoparticles in (bio)medical applications, cytotoxicity and cellular uptake of bacterial magnetosomes by mammalian cells have so far not comprehensively been studied. Furthermore, in most studies varying cell lines were investigated, which differ in their sensitivity to magnetosome treatment, and assays are applied that assess different metabolic activities. Thus, collected data are difficult to compare across the published studies and different research groups, and there is still no comprehensive evaluation that includes cytotoxicity, potential effects on cell proliferation as well as the interaction and uptake of the particles by mammalian cells.

Recently, our group established and characterized isolation procedures for bacterial magnetosomes from *M. gryphiswaldense* combining magnetic separation and density-based ultracentrifugation.[13,14,29] The resulting, highly purified magnetosome suspensions were homogeneous and nearly free of impurities such as cell debris or polyhydroxybutyrate (PHB). As for many envisioned biomedical applications the particle suspension would be directly applied to mammalian cells or injected into the body, potential cytotoxic effects were furthermore investigated. For that purpose, purified magnetosomes were incubated with mammalian cells for 24 h. The viability rates for the tested FaDu (squamous hypopharyngeal carcinoma) cell line confirmed biocompatibility for magnetosome concentrations up to ~200 μg mL^{-1}, and for higher particle amounts (390 μg mL^{-1}) a moderate viability (≥69%) was observed.[29] However, it so far remained unclear if isolated magnetosomes remain stable upon prolonged incubation in physiological fluids. The latter usually represent complex mixtures of organic compounds, such as amino acids or sugars, and varying concentrations of salt that might affect the state of the surrounding magnetosome membrane (*e.g.* charge patches or hydrophobicity), potentially causing the formation of unstable agglomerates. The colloidal stability in such media is therefore an important prerequisite for further studies on effects of the magnetosome-treatment on cell viability and proliferation.

In our study, we therefore first systematically assessed the stability of magnetosomes when incubated in different complex cell culture media at various Fe concentrations, thereby defining conditions suitable for *in vitro* investigations. We then evaluated biocompatibility and the interaction and uptake of isolated magnetosomes by mammalian cells. As many cell lines are assumed to differ in their sensitivity,[6] we tested a set of four different cell lines including primary cells as well as carcinoma cells with regard to cell viability upon the treatment with varying magnetosome concentrations. A representative carcinoma cell line, FaDu, was finally chosen to further evaluate magnetosome–cell interactions. First, the cellular uptake of the particles upon prolonged incubation times was studied. Next, for increasing particle amounts, potential effects of the magnetosome-treatment on cell proliferation were monitored by real-time analyses. Finally, we investigated magnetosome-loading of FaDu cells upon short-term incubation to allow for subsequent magnetic cell sorting. The magnetization of the cancer cells (due to increased interactions with the magnetosomes) might therefore be of great importance for the application of magnetosomes *e.g.* as targeting agents, in particular for circulating tumor cells (CTCs).[30]

Overall, our study critically examines the suitability of purified bacterial magnetosomes for future biomedical applications from different angles, thereby comprehensively assessing effects on cell proliferation, viability (*i.e.* metabolic activity) and cell death. The obtained overall picture of magnetosome biocompatibility is

furthermore complemented by in-depth evaluation of the interaction of isolated particles with a representative cancer cell line (FaDu), including magnetic labelling, cellular uptake and subcellular localization. We therefore firmly believe that our collected data might soon pave the way for the future use of purified bacterial magnetosomes in real-world applications.

Experimental section

Cell culture

For assessing the cytotoxicity of isolated magnetosomes, four different mammalian cell lines were tested (Table S1†). In order to provide optimal growth conditions and to ensure that potential impairments in cell viability and proliferation are solely due to magnetosome treatment, cultivation was performed as recommended by the suppliers for the respective cell lines.

The adherent squamous hypopharyngeal carcinoma cell line FaDu (HTB-43, ATCC, Manassas, VA, USA)[31] was cultured in Dulbecco's Modified Eagle's Medium (DMEM) supplemented with 10% (v/v) Fetal Bovine Serum (FBS) (Sigma-Aldrich, Steinheim, Germany). The adherent non-small cell lung carcinoma cell line HCC78 was obtained from DSMZ (ACC 563, Braunschweig, Germany). The cell line was established from a pleural effusion from a 65 year old man.[32] HCC78 cells were cultured in RPMI1640 medium with GlutaMAX-I (RPMI) and 10% (v/v) FBS. Primary human placental pericytes (hPC-PL; PromoCell GmbH, Heidelberg, Germany) are mesenchymal-like cells often found in association with small blood vessels. These cells were initially cultivated in Pericyte Growth Medium (PGM; PromoCell GmbH, Heidelberg, Germany) according to the purchaser's recommendations and then adapted to DMEM supplemented with GlutaMAX-I and 10% (v/v) FBS. Pericyte cultures were used in passages 6 to 10. The trophoblast cell line BeWo (ACC 458, DSMZ, Braunschweig, Germany) is derived from a choriocarcinoma.[33] The cell line was initially cultivated in Ham's F12 supplemented with 15% (v/v) FBS and 2 mM L-glutamine and then adopted to DMEM supplemented with GlutaMAX-I and 15% (v/v) FBS.

All cell lines were cultivated in a cell culture incubator (37 °C, 5% CO_2, 95% relative humidity). The cells were sub-cultured at a confluence of 80–90%. Therefore, the medium was removed and the cell cultures were washed two times with 5 mL phosphate buffered saline (PBS). Afterwards, 3 mL trypsin-ethylenediaminetetraacetate (EDTA) 0.05% solution was added and the cell cultures were incubated for 3 min at 37 °C until the cells detached from the culture flask. Cell suspensions were diluted in appropriate ratio by adding fresh medium. In regular intervals cell cultures were tested regarding mycoplasmic contaminations using the commercial PCR-based Venor Gem mycoplasma detection kit (Sigma-Aldrich Chemie GmbH, Steinheim, Germany).

Preparation of FaDu-NR cells

In order to fluorescence label FaDu cells were transduced with the IncuCyte™ NucLight Lentivirus Red Reagent (Essen BioScience, Göttingen, Germany) three times and subsequently selected against puromycin (2 μg mL^{-1}) enabling a stable nuclear labelling by nuclear-restricted mKate2 expression, hereinafter named FaDu NucLight Red (FaDu-NR).

Cultivation of *M. gryphiswaldense*

The wildtype (WT) strain of *M. gryphiswaldense*[34] was grown in modified flask standard medium (FSM) under moderate shaking (120 rpm) at 30 °C.[35] Cultivation was performed in 10 L flasks, and magnetite formation was ensured by applying a headspace-to-liquid ratio of ~1 : 4 with air in the headspace. Oxygen concentrations declined from high initial levels in the medium with increasing cell numbers, eventually reaching low dissolved oxygen concentrations (*i.e.* microoxic conditions), thereby inducing magnetite synthesis.[36] Cells of the late exponential phase were harvested by centrifugation (9000*g*, 4 °C, and 20 min). The cell pellets were washed with 20 mM HEPES, 5 mM EDTA, pH 7.2 and stored at −20 °C until further use.

Magnetosome isolation and purification

Extraction/purification of magnetosomes was performed as previously described.[14,29] Briefly, cell pellets of *M. gryphiswaldense* were resuspended in 50 mM HEPES, 1 mM EDTA, pH 7.2, prior to disrupting the cells by 3–5 passages through a microfluidizer system (M-110L, Microfluidics Corp., Westwood, MA, USA). The obtained crude extracts were passed through a MACS magnetic-separation column (5 mL; Miltenyi Biotec, Bergisch Gladbach, Germany), which was placed between two neodymium-iron-boron magnets (each 1.3 T). After loading the extracts onto the column, the latter was washed with 50 mL 10 mM HEPES, 1 mM EDTA, pH 7.2, followed by 50 mL high-salt buffer (10 mM HEPES, 1 mM EDTA, 150 mM NaCl, pH 7.2) to remove electrostatically bound cellular compounds, and again 50 mL 10 mM HEPES, 1 mM EDTA, pH 7.2. Finally, the magnets were removed and the magnetosomes retained in the column were eluted with H_2O_{dd}. Residual cellular contaminants still present in the magnetosome suspension were removed by an ultracentrifugation step. The eluted magnetosomes were loaded onto a sucrose cushion (60% w/v in 10 mM HEPES, 1 mM EDTA, pH 7.2) and centrifuged for 2 h at 200 000*g* and 4 °C. The magnetosome pellet formed upon centrifugation was subsequently resuspended in 10 mM HEPES, 1 mM EDTA, pH 7.2, and the particle dispersions were stored in Hungate tubes under a nitrogen atmosphere at 4 °C until further use.

Determination of iron concentrations

Iron contents of suspensions of isolated magnetosomes were determined by atomic absorption spectroscopy. Magnetosomes were pelleted, resuspended in 1.0 mL 69% nitric acid and digested at 98 °C for 3 h. Samples were filled up with H_2O_{dd} to a final volume of 3.0 mL and subsequently analyzed using an Analytik Jena contrAA300 high-resolution atomic absorption spectrometer (Analytik Jena, Jena, Germany) equipped with a 300 W xenon short-arc lamp (XBO 301, GLE, Berlin, Germany) as continuum radiation source. The equipment included a compact high-resolution double monochromator (consisting

of a prism pre-monochromator and an echelle grating monochromator) and a charge-coupled device (CCD) array detector with a resolution of about 2 pm per pixel in the far ultraviolet range. Measurements were performed at a wavelength of 248.3 nm using an oxidizing air/acetylene flame. The number of pixels of the array detector used for detection was 3 (central pixel 1). All measurements were carried out in quintuplicates on three technical replicates.

Fluorescent labelling of isolated magnetosomes

DyLight 488 Amine-Reactive Dye (NHS ester-activated derivative of high-performance DyLight 488; Thermo Scientific, Waltham, MA, USA) was used for fluorescent labelling of WT magnetosomes. Isolated particles (24 μg Fe) in 162 μL 50 mM $NaHCO_3$, pH 9.0 were supplemented with 1.15–4.6 μL DyLight 488 NHS ester (10 mg mL^{-1} in dimethylformamide) and incubated in the dark for 2 h at 16 °C. Excess dye was removed by extensive washing steps in which the particles were pelleted by centrifugation (4000*g*, 15 min) and after discarding the supernatant, resuspended in 200 μL 10 mM HEPES, 1 mM EDTA, pH 7.2. Success of the labelling reaction was confirmed by fluorescence microscopy (Fig. S1†) using an Olympus IX81 microscope equipped with a Hamamatsu Orca AG camera as previously described.[36]

Transmission electron microscopy

For transmission electron microscopy (TEM) analysis, FaDu cells were grown on 22 × 22 mm glass coverslips and incubated with WT magnetosomes corresponding to an iron concentration of 5 μg cm^{-2}, 25 μg cm^{-2} or 50 μg cm^{-2} for 24 h. Cells were prefixed in culture medium with 2.5% glutaraldehyde, pH adjusted to 7.2, for 20 min at 37 °C. Cells were then fixed in 0.1 M HEPES, 4 mM $CaCl_2$, 2.5% glutaraldehyde (Serva Electrophoresis, Heidelberg, Germany), 2.5% formaldehyde (Science Services, Munich, Germany), pH 7.2 for 1 h at room temperature plus 4 h at 4 °C. Fixative was replaced twice. Cells were post-fixed with 1% OsO_4 for 45 min at room temperature and then incubated in 1% uranyl acetate overnight at 4 °C. Between each step the samples were washed 3–4 times for 5 min each in 0.1 M HEPES, 4 mM $CaCl_2$, pH 7.2. Dehydration of the samples in ethanol, infiltration with Epon (Serva Electrophoresis) and flat embedding was done by standard procedures.[37] Ultrathin serial sections (~60–70 nm) were cut with a diamond knife (type ultra 35°; Diatome, Biel, Switzerland) on an EM UC6 ultramicrotome (Leica, Wetzlar, Germany) and mounted on single-slot Pioloform-coated copper grids (Plano, Wetzlar, Germany). Sections were stained with uranyl acetate and lead citrate[38] and viewed with a JEM-2100 or JEM-1400Plus transmission electron microscope (JEOL, Tokyo, Japan) operated at 80 kV. Micrographs were taken at the JEM-2100 using a 4000 × 4000 charge-coupled device camera (UltraScan 4000; Gatan, Pleasanton, CA) and Gatan Digital Micrograph software (version 1.70.16.). Image brightness and contrast were adjusted and figures assembled using Adobe Photoshop 8.0.1 and GIMP (GNU Image Manipulation Program) 2.10.18.

For TEM of isolated magnetosomes, specimens were directly deposited onto carbon-coated copper grids (Science Services, Munich, Germany). Particles were negatively stained with 2% uranyl acetate. TEM was performed on a CEM 902A (Zeiss, Oberkochen, Germany) with an acceleration voltage of 80 kV. Images were taken with a Gata Erlangshen ES500W CCD camera.

Dynamic light scattering (DLS) measurements

The colloidal stability of purified magnetosomes in various buffer solutions and cell culture media was investigated by using dynamic light scattering (DLS). Thereby it could be ensured that the isolated particles stay stably in suspension during incubation with mammalian cells and did not irreversibly form agglomerates. Magnetosome suspensions were pelleted by centrifugation (4000*g*, 15–30 min, 4 °C) and resuspended in cell culture media (RPMI, DMEM) or buffer solutions (Hank's Balanced Salt Solution, HBSS) at a final concentration of 50, 100, 200 or 400 μg Fe mL^{-1}. Suspensions were subsequently incubated for 12, 24 or 48 h, and DLS was used to determine hydrodynamic diameters and to monitor the formation of potential agglomerates. Measurements were performed in quintuplicates on three biological replicates (n_{total} = 15) using a Zetasizer Nano (Malvern, UK) and 70 μL UV micro cuvettes (Brand, Wertheim, Germany). The evaluation software provided by the supplier (Malvern Zetasizer Software 7.13) is based on the Cumulant method and uses the Stokes–Einstein-equation for size determination.

PrestoBlue cytotoxicity assay

After incubation with different particle amounts, the viability of the magnetosome-treated FaDu, BeWo, HCC78 or hPC-PL cell cultures was analyzed using the PrestoBlue assay (Invitrogen, Karlsruhe, Germany). It is based on the ability of metabolically active, vital cells to reduce the non-fluorescent resazurin to the fluorescent resorufin.

For that purpose, 15 000 (FaDu, BeWo, HCC78) or 25 000 (hPC-PL) cells per well in 72 μL of the respective growth medium supplemented with penicillin/streptomycin (P/S) (10 000 U mL^{-1}, 10 000 μg mL^{-1}) were seeded into a black-walled 96-well plate and cultivated for 24 h. Subsequently, 18 μL magnetosome suspension with final iron concentrations of 5 μg cm^{-2}, 25 μg cm^{-2}, 50 μg cm^{-2}, and 100 μg cm^{-2} (diluted with the respective growth medium supplemented with P/S) were added. For the untreated negative control, 18 μL of the respective growth medium supplemented with P/S were applied. As a positive control, 18 μL of Triton X-100 were used, resulting in a final concentration of 0.02% (w/v). Incubation with the different treatments was performed for 24 or 48 h in a cell culture incubator (37 °C, 5% CO_2, 95% relative humidity). After the incubation, 10 μL of PrestoBlue reagent was added to each well and the plate was incubated for 30 min in a cell culture incubator at 37 °C. The plate was placed for 5 additional minutes on a Magnetic-Ring Stand 96-well plate in the dark in order to prevent disturbances during fluorescence measurement by the magnetosomes. The fluorescence (ex/em: 560/600 nm) was

measured with the CLARIOstar microplate reader (BMG LABTECH GmbH, Ortenberg, Germany).

SYTOX staining

In order to study cytotoxic effects of magnetosomes, SYTOX™ staining was performed. SYTOX™ red dead cell stain (Invitrogen, Karlsruhe, Germany) is a membrane-impermeable DNA dye, which is able to enter cells with compromised cell membranes. When binding to DNA, the dye undergoes significant fluorescence enhancement, leading to a selective staining of dead cells when excited with 633/635 nm red laser light, which can be detected at 658 nm.

In scope of evaluating potential cytotoxic effects of magnetosomes, the respective cell lines (BeWo, FaDu, HCC78, and hPC-PL; each 500 000 cells) were seeded into 6-well plates and cultivated overnight. After incubation with the indicated concentrations of magnetosomes for 24 or 48 h, the cells including the supernatant were harvested by treatment with Accutase (Sigma-Aldrich, Merck, Darmstadt, Germany). After washing twice with PE (2 mM EDTA in PBS), the cells were resuspended in 500 μL of a 2.5 nM SYTOX™ red dead cell stain solution and incubated at 4 °C in the dark for 15 min. For control purposes, an unstained sample as well as samples containing only magnetosomes were prepared simultaneously. Furthermore, a positive control using 0.1% Triton X-100 was included. The samples were measured instantly without performing another washing step, because the dye binds in equilibrium with the DNA and therefore external concentration has to be maintained (FACSCalibur, Becton-Dickinson, Heidelberg, Germany).

Confocal laser scanning microscopy

Subconfluent FaDu cell cultures were incubated with 10 or 25 μg Fe cm^{-2} DyLight488-labeled WT magnetosomes (green) for 24 h. Interaction and uptake were analyzed with the confocal laser scanning microscope LSM 510 META (Carl Zeiss, Jena, Germany) and the appendant software ZEN 2012 SP1 blue edition (version 8.1). The cytoskeleton was visualized with phalloidin-AF633 (red) (Invitrogen, Karlsruhe, Germany) and the nuclei with Hoechst 33258 (blue) (Invitrogen, Karlsruhe, Germany).

Prussian blue staining

For studying the interaction of magnetosomes with FaDu cells, the Prussian blue staining was used as described previously by Schlorf *et al.*[39] Thereby, potassium ferrocyanide trihydrate forms a blue complex with Fe(III)-ions derived from magnetosomes. One day prior to the experiment, 400 000 FaDu cells were seeded onto coverslips in 24-well plates. After incubation with magnetosomes, cells were washed twice with PBS before fixation using 10% formalin solution for 15 min at RT. The staining was performed using 2% (w/v) potassium ferrocyanide trihydrate in 1 M HCl for 10 min at 37 °C. Afterwards, the cell cytoplasm was counterstained using DiffQuick Stain solution (Labor + Technik Eberhardt Lehmann, Berlin, Germany) and the coverslips were analyzed instantly using the light microscope Axiovert 25, the camera AxioCam HRc and the software AxioVision SE64 4.9 (Carl Zeiss GmbH, Jena, Germany).

Live cell imaging and analysis

150 000 FaDu-NR cells were seeded in 96-well plates and cultivated for 24 h at 37 °C, 5% CO_2 in a humidified atmosphere. Cells were incubated with 5, 25, 50, 100 μg cm^{-2} magnetosomes. Untreated FaDu-NR cells and cells incubated with HEPES buffer served as positive control. Cell cultures treated with 0.1% (v/v) Triton X-100 or 50 μg cm^{-2} polyethylene imine (PEI) coated nanoparticles (micromod Partikeltechnologie, Rostock, Germany) were used as negative control. The latter represent magnetite core–shell nanoparticles of ~150 nm in diameter exhibiting a cationic surface charge. Positively charged nanoparticles have been shown to exert toxic effects to mammalian cells, depending on net charge, composition of the shell and particle concentration applied. For instance, the viability of human brain microvascular endothelial cells (HBMEC) was drastically reduced upon incubation with PEI-coated nanoparticles, and concentration >25 μg mL^{-1} caused a high number of cell death events.[40,41]

The number of red-fluorescent nuclei as a measure for the number of vital cells over a time period of 44 h was determined with the IncuCyte™ ZOOM live cell analyzer (Essen Bioscience, Ann Arbor, MI, USA) and denominated as "red object count". The values at the starting point (0 h) were set "1" and the measurements during the incubation period were related to this value.

Three-dimensional growth

FaDu-NR cells were incubated with 25 μg cm^{-2} magnetosomes in DMEM + 10% FBS for 24 h. The cells were detached with Trypsin–EDTA, centrifuged and resuspended to a final volume of 1×10^6 cells per mL. The cell suspension was applied to a MACS MS column (Miltenyi Biotec). The cells in the flow-through and the retained cell fraction were counted. 5000 cells per well from both fractions as well as FaDu-NR cells without magnetosome incubation were seeded into a 96-well u-bottomed microwell plate (Greiner Bio-One, Frickenhausen, Germany) and centrifuged at 200*g* for 5 min to allow the cells to sediment at the bottom of the well. Spheroid formation was allowed and monitored in an IncuCyte™ ZOOM live cell analyzer (Essen Bioscience) in a humidified atmosphere at 37 °C, 5% CO_2 for 96 h.

Magnetic separation

Cells from standard FaDu cell cultures were prepared by applying 1× Accutase (Merck, Darmstadt, Germany) in order to preserve the cell surface structure. Leukocytes were enriched from the peripheral blood of a healthy volunteer by erythrocyte lysis and subsequent centrifugation. 1×10^6 FaDu cells or 2.5×10^6 leukocytes were incubated with magnetosomes (10–100 μg Fe mL^{-1}) for 8 min independently. The suspensions were subsequently separated using MS magnetic columns (Miltenyi Biotec) and a SuperMACS device (Miltenyi Biotec). Cells from the flow-through (negative fraction) and cells retained in the

magnetic field (positive fraction) were counted (Coulter Counter Z2, Beckman–Coulter, Brea, CA, USA). 125 000 FaDu-NR cells (5%) were mixed with 2.5 × 10^6 leukocytes (95%) and treated with magnetosomes (25 μg Fe mL^{-1}) for different incubation times (up to 20 min). The mixed cell suspensions were applied to the SuperMACS device and separated magnetically. Cells from the positive and negative fraction were counted. The portion of FaDu-NR cells in the negative and the positive fraction was determined by flow cytometry using a FACSCalibur (Becton-Dickinson, Franklin Lakes, NJ, USA).

Statistical analyses

Group data are presented as mean ± standard deviation, n indicates the number of independent experiments. SPSS Statistics software (version 26) was used for one-way ANOVA tests with 95% confidence intervals followed by a multiple comparison test and correction according to Tukey.[42] Differences are considered as statistically significant for $p < 0.05$ (*), $p < 0.01$ (**), or $p < 0.001$ (***) as specified in the figure legends.

Results

Colloidal stability of isolated magnetosomes in physiological fluids

As prerequisite for cell culture experiments, we investigated the colloidal stability of the particles in physiological fluids (*i.e.* different buffer solutions and cell culture media) to ensure optimal particle dispersion and membrane integrity. Magnetosomes were isolated from disrupted bacterial cells according published procedures[14,29] and incubated in HBSS (with or without additional Ca^{2+} and Mg^{2+}), RPMI, or DMEM (supplemented with different FBS concentrations) for 12, 24 or 48 h at defined iron concentrations. For all tested conditions, DLS revealed hydrodynamic diameters <800 nm (Fig. S2†), indicating a general suitability for cellular uptake.[6] Partially, a trend towards increased sizes with prolonged incubation times was observed, in particular for higher magnetosome concentrations (400 μg Fe mL^{-1}). This was essentially confirmed by TEM micrographs, in which chains of up to 600 nm in length were visible, as well as agglomerates of up to 500 nm in diameter (Fig. S3†).

Interestingly, for incubation in RPMI at increasing FBS concentrations, the hydrodynamic diameters of magnetosomes/particle agglomerates decreased. Thus, for 5 or 10% FBS, nearly no agglomerates in the size range from 400 to 650 nm could be detected (as illustrated in Fig. S2†). This is furthermore supported by TEM analyses (Fig. S3†), which revealed the formation of longer chains for 2% FBS. In contrast, for 5 or 10% FBS only smaller agglomerates/chains or individually dispersed magnetosomes were observed, again confirming the results of the DLS measurements. These observations might be explained by the formation of a protein corona on the magnetosome surface, as it has been described *e.g.* by Gräfe and co-workers for polyethyleneimine (PEI)-coated magnetic nanoparticles.[43] In the mentioned study, the latter were incubated in cell culture medium with increasing FBS concentrations. Thereby, the formation of a protein corona was observed, and the amount of corona proteins was increased with the amount of FBS in the incubation medium. Whereas with lower FBS concentrations medium-sized proteins of molecular weights between 30 kDa and 100 kDa could be found within the protein corona, for nanoparticles incubated within higher FBS concentrations the fraction of corona proteins of 30 kDa and less increased. Moreover, the protein corona reduced the interaction of the nanoparticles (*i.e.* adhesion to the cell surface and particle uptake) with human brain microvascular endothelial cells (HBMEC) even after short-term incubation of 30 min.[43] Similarly, it can be assumed that during incubation with FBS-containing media, a protein corona is formed that surrounds individual magnetosomes, and differing FBS concentrations might affect the composition of the protein shell. Thus, increased FBS concentrations of 5 or 10% might not only facilitate the formation of such a shell but also increase its thickness. At such FBS concentrations, particle–particle interactions might be influenced or even shielded by corona proteins to some extent, leading to smaller aggregates and individually dispersed magnetosomes as indicated in Fig. S3B and C.† Moreover, the magnetosomes showed different agglomeration behavior when incubated in RPMI and DMEM media (each supplemented with 10% FBS). This is obvious from TEM micrographs (Fig. S3C and D†) as well as hydrodynamic diameters of agglomerates determined by DLS. Whereas for magnetosomes incubated in RPMI + 10% FBS only smaller agglomerates were detected, aggregation tendencies were clearly increased in DMEM + 10% FBS, and size classes >500 nm could be detected. The formation of a protein corona is strongly influenced by the surrounding environment and factors such as the ionic strength, pH values and the presence of plasma proteins.[44,45] Thus, the composition of the cell culture medium plays a crucial role in protein adsorption to the nanoparticle surface.

Protein–nanoparticle interactions were found to be differentially mediated by RPMI and DMEM cell culture media, and protein coating occurred at different rates and dynamics.[46] The composition of the culture media might therefore explain the observed agglomeration behavior. For instance, for DMEM the overall content of amino acids is increased, as well as the amount of sugar (D-glucose).[47] Although these effects will require further investigations, our data so far clearly indicate that magnetosome concentrations up to 400 μg Fe mL^{-1} are stable in DMEM or RPMI cell culture media (supplemented with up to 10% FBS) for at least 48 h and thus, can be applied for further studies on biocompatibility and interactions with mammalian cells.

Magnetosomes exhibit no cytotoxic effects on mammalian cells

In order to obtain a comprehensive, clear picture of potential cytotoxic effects of isolated magnetosomes, different mammalian cell lines were treated with varying particle concentrations, and different assays were applied to assess viability and cell death rates. Besides primary human placental pericytes (hPC-

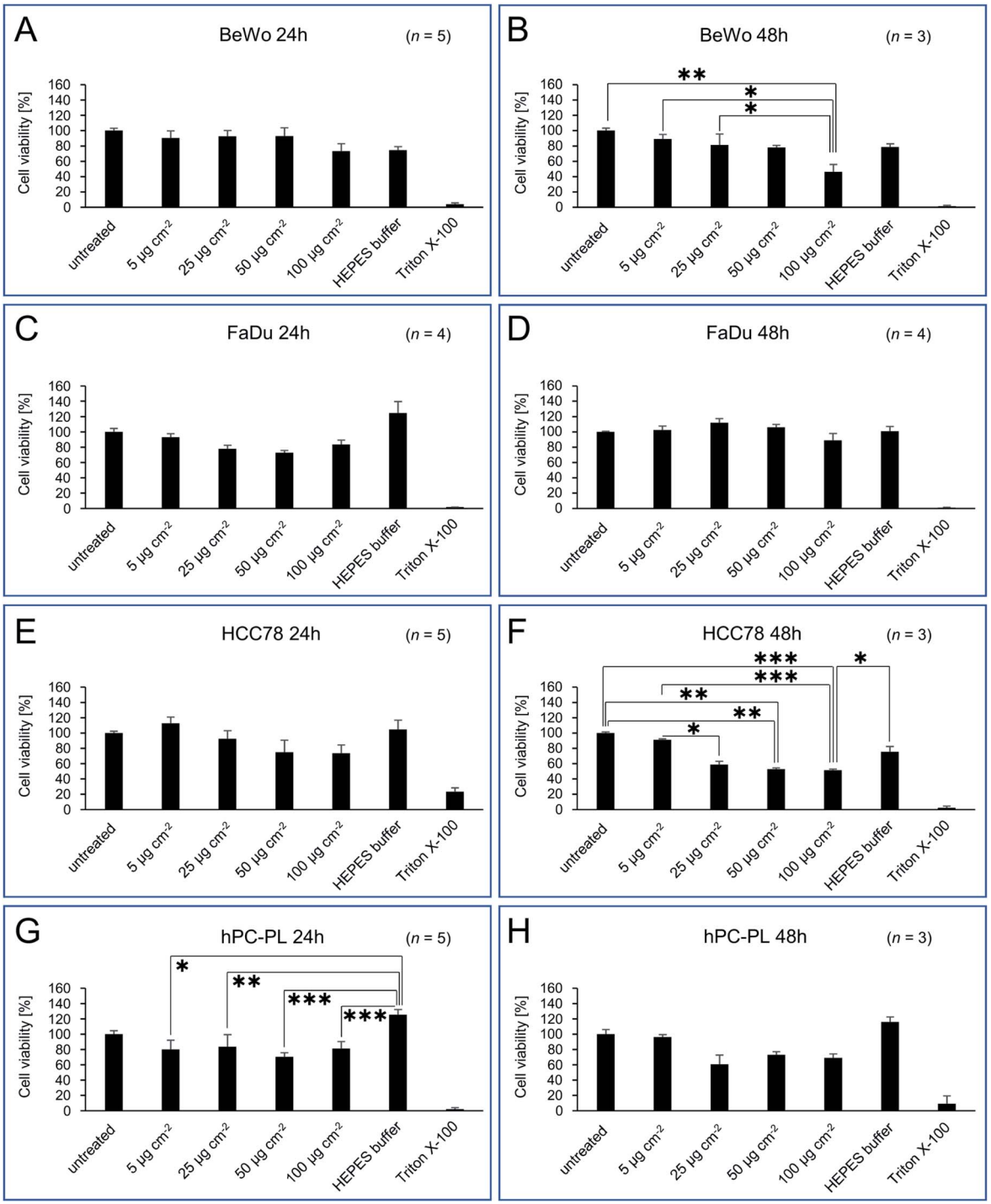

Fig. 2 Cell viability of BeWo (A/B), FaDu (C/D), HCC78 (E/F) and hPC-PL (G/H) cell lines incubated with different concentrations of isolated magnetosomes. PrestoBlue assays were performed to assess potential cytotoxic effects of the indicated amounts of isolated magnetosomes when added to the respective cell line (incubation for 24 or 48 h). Viability values are given as percentage of the value obtained for untreated cells (negative control). Cells incubated with 0.02% Triton X-100 served as positive control. As illustrated by the bar charts, for 24 h incubation time magnetosome concentrations up to 50 μg cm^{-2} (194.4 μg mL^{-1}) were considered to be biocompatible, with viability values ≥69% (classified as moderate viability; EN ISO 10993-5:2009).[48] For 48 h of incubation, trends towards decreasing viability rates were observed, however, sensitivity to magnetosome treatment differed depending on the tested cell line, with FaDu exhibiting the highest viability rates (>90% for 100 μg Fe cm^{-2}). Number of biological replicates (*n*) as indicated, statistically significant differences are denoted as follows: $p < 0.05$ (*), $p < 0.01$ (**), $p < 0.001$ (***). Statistical analysis and *p*-values are provided in Table S2.† Please note, that statistically significant differences to Triton X-100 (which applies to the majority of samples tested) are not included in the figure, but listed in Table S2.†

PL) representing a non-transformed cell type, we used epithelial-type tumor cell lines, namely FaDu originated from a hypopharyngeal carcinoma,[31] and the non-small cell lung carcinoma cell line HCC78.[32] In addition, the human choriocarcinoma cell line BeWo[33] was included, which is an *in vitro* model for trophoblasts and can be differentiated into syncytiotrophoblasts. After incubation for 24 or 48 h with different particle concentrations (5, 25, 50 or 100 μg Fe cm^{-2}, which equals 19.4, 97.2, 194.4 and 388.9 μg Fe mL^{-1}), PrestoBlue assays were performed to evaluate the cell viability. Untreated cells and cells treated with 0.02% (w/v) Triton X-100 served as controls. As the magnetosomes themselves led to low fluorescence/luminescence signals, a background correction was performed. For direct comparison, treated cells were normalized to an untreated control, which was set to 100% of viable cells. Besides the FaDu cell line, concentration-dependent effects on cell viability were observed (as shown in Fig. 2). In general, for 24 h incubation time, magnetosome concentrations up to 50 μg cm^{-2} (194.4 μg mL^{-1}) were considered to be biocompatible, with viability values ≥69% (classified as moderate viability according to EN ISO 10993-5:2009).[48] Thereby, the tested cell lines differed in their sensitivity to magnetosome treatment. Whereas for BeWo (Fig. 2A) and hPC-PL (Fig. 2G) viability fluctuated between 70 and 90%, the FaDu cell line seemed to be more robust, with values >80% for all applied magnetosome concentrations (Fig. 2C). In contrast, for HCC78 a trend towards slightly decreasing viability rates was observed, however, even for the highest tested concentration (100 μg cm^{-2} or 388.9 μg mL^{-1}) cell viability was still >70% (Fig. 2E). Prolonged magnetosome treatment up to 48 h further reduced cell viability for all cell lines investigated, and an overall trend to decreasing values was observed. Again, HCC78 turned out to be more sensitive to magnetosome treatment, and viability dropped to ~50% for 50 or 100 μg cm^{-2} magnetosomes (Fig. 2F). Similar, albeit less pronounced effects were observed for BeWo and hPC-PL, with the highest tested magnetosome concentration of 100 μg Fe cm^{-2} reducing cell viability to 60–70% (Fig. 2B and H). As observed before, FaDu cells exhibited the highest viability rates. Thus, even for 100 μg Fe cm^{-2} still values >90% were observed (Fig. 2D). Overall, our collected data suggest a general biocompatibility of magnetosomes for incubation times up to 24 h. Although the tested cell lines differed in their sensitivity to magnetosome treatment, viability rates argue for moderate to good viability under the applied conditions.

Besides the magnetosome treatment, we also observed a visible but not statistically significant influence of the HEPES buffer *per se* on the cell viability. Thereby, for FaDu and hPC-PL a positive influence on viability was observed, whereas for BeWo cells viability seemed to be reduced after 24 or 48 h, respectively.

HEPES is a buffer commonly used for *in vitro* cultivation of established cell lines as well as primary cells. It increases buffer capacity and allows to control pH in the physiological range.[49] This is of special importance for mesenchymal cells (*e.g.* pericytes) and thus, may contribute to the elevated viability of hPC-PL cells. Taking into account the small reaction volume (100 μL) during the PrestoBlue cytotoxicity assay, the addition of HEPES with a final concentration of 2 mM may allow a better maintenance of a physiological pH for at least 24 h and thus, explain the lightly elevated values for HCC78 and FaDu cell cultures. The observed reduction of BeWo viability in the presence of HEPES might be due to toxic effects. Suppliers of HEPES point out that this substance should not be used in high concentrations because of toxic effects on cell cultures. The recommended final concentration of HEPES in cell culture media is 10–25 mM, thus 2 mM HEPES in our setting seems to be not responsible for the reduced viability of BeWo cells.

So far, the applied PrestoBlue assays had provided only qualitative data on the viability of the respective cell lines when incubated with magnetosomes, but no information on the total number of vital cells. Therefore, we performed SYTOX assays followed by flow cytometry analysis for (semi-)quantitative determination of death rates of individual cells. The different cell lines BeWo, FaDu, HCC78, or hPC-PL were incubated with 100 μg cm^{-2} magnetosomes for 24 or 48 h. As expected, for the positive control (cells treated with 0.1% Triton X-100) cell death rates ≥90% were observed. The obtained cell death rates (Table S3†) were finally used to calculate the corresponding cell viability values (illustrated in Fig. 3) to allow for direct comparison with the PrestoBlue data (Fig. 2). The values for the

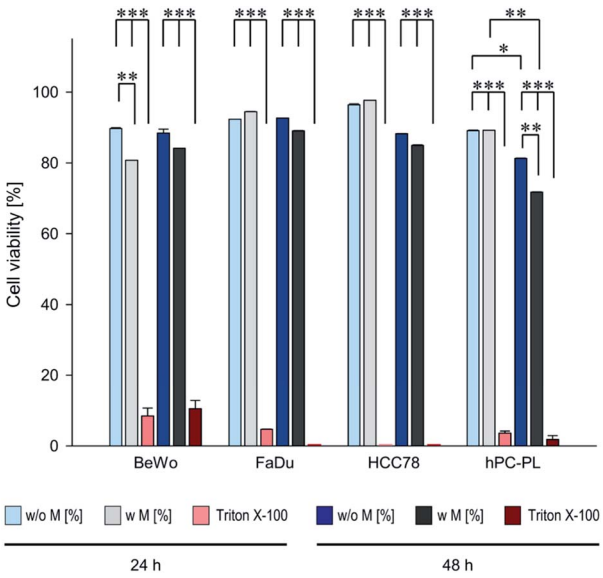

Fig. 3 Viability rates of magnetosome-treated BeWo, FaDu, HCC78 and hPC-PL cells determined by SYTOX™ staining assay. 500 000 cells of the respective cell lines were incubated with isolated magnetosomes (100 μg cm^{-2}) for 24 or 48 h ("w M"). Afterwards, cell death rates were determined using the SYTOX™ assay followed by flow cytometry analysis. Untreated cells ("w/o M") and cells treated with 0.1% Triton X-100 served as controls. The obtained values (provided in Table S3†) were subsequently taken to calculate cell viability rates. Incubation with Triton X-100 resulted in viability rates ≤10%. Whereas for the magnetosome-treated FaDu and HCC78 cells viability was comparable to the corresponding untreated fractions, the more sensitive BeWo and hPC-PL exhibited a slight but partially significant viability decrease, which is in agreement with the results from PrestoBlue assays (Fig. 2). Data are presented as mean ± standard deviation, $n \geq 2$. Differences considered as statistically significant are specified as follows: $p < 0.05$ (*), $p < 0.01$ (**), or $p < 0.001$ (***). Statistical analysis is provided in Table S4.†

magnetosome incubated cell cultures were mostly comparable to the untreated cells after 24 h. Thereby, for FaDu, HCC78 and hPC-PL cell viability values ≥89% were detected. Only for the BeWo cell line a slightly increased portion of dead cells was observed upon magnetosome incubation (viability 80.7%, untreated BeWo 89.7%). After 48 h, however, treated cell lines exhibited a clear proportion of dead cells. Whereas for BeWo, FaDu and HCC78 cell viability values were only marginally diminished compared to the untreated fractions, a more pronounced effect was observed for hPC-PL (viability 71.8%, untreated hPC-PL 81.3%). These data are consistent with the results of the PrestoBlue assay (Fig. 2), which indicated a high cell viability (>70%) for all tested cell lines at the highest particle concentration after 24 h; however, upon prolonged magnetosome treatment (48 h) cell conditions were affected to some extent.

Magnetosome uptake and subcellular localization

For many envisioned magnetosome-based applications, such as counting and enrichment of circulating tumor cells from peripheral blood,[50–52] evaluation of cell–particle interactions are of great importance. For further analysis, in particular investigations regarding magnetosome uptake and the fate of the particles after internalization, the FaDu cell line was chosen, because of their robustness with regard to magnetosome incubation in our previous investigations.[29] Furthermore, the latter has proven to be well-suited for investigations regarding the cytotoxicity and uptake of nanoparticles.[53] When incubated with chitosan-based nanoparticles, FaDu cells exhibited viability values and cellular uptake rates that were comparable to those of the HeLa-derivative Hep-2 cells, a cell line that has often been used for studies on cytotoxicity and uptake of nanoparticles.[54]

First, we investigated magnetosome internalization by using confocal laser scanning microscopy (cLSM). For that purpose, subconfluent FaDu cells were incubated with fluorescent, DyLight488-labelled magnetosomes (10 or 25 μg Fe cm^{-2}) for 24 h. For both tested particle concentrations cLSM analysis revealed distinct fluorescence signals indicating magnetosome internalization. The particles showed no organized co-localization with cytoskeletal structures but accumulated as distinct fluorescent spots in close proximity to the nuclei, suggesting a typical endolysosomal signature (Fig. 4). After Prussian blue staining of the respective cLSM preparations, a typical bluish stain was visible, indicating the presence of ferric iron (data not shown). These signals co-localized with the fluorescence signals in cLSM, thereby confirming particle uptake. Fluorescence microscopy essentially confirmed these observations (Fig. S4†).

In order to obtain a more detailed picture on the magnetosome uptake and the subcellular localization of the particles, we incubated FaDu cells with unlabelled WT magnetosomes, fixed the cells and, after dehydration and plastic embedding, cut ultrathin serial sections of the preparations for subsequent TEM analysis. Here, in a variety of cells vesicle-like structures were visible that contained high amounts of particles (Fig. 5A, B and S5†). These vesicles (up to 15 per cell) were located within the cytoplasm, partially in direct vicinity to the nuclei, and were surrounded by membranous structures (Fig. S5†). In addition, even in dividing cells such vesicles could be found (Fig. 5B). Our data therefore suggest endocytosis-based magnetosome internalization, with the particle stored in lysosomal, vesicle-like structures. Furthermore, magnetosomes were still visible in the area surrounding the cells. Here, agglomerates and smaller particle chains could be observed, and variations in electron density/contrast suggest intact magnetosome membranes (Fig. 5A, inset ii).

Effects on cell proliferation

In TEM analyses, internalized magnetosomes were observed even in dividing FaDu cells. In order to assess potential effects

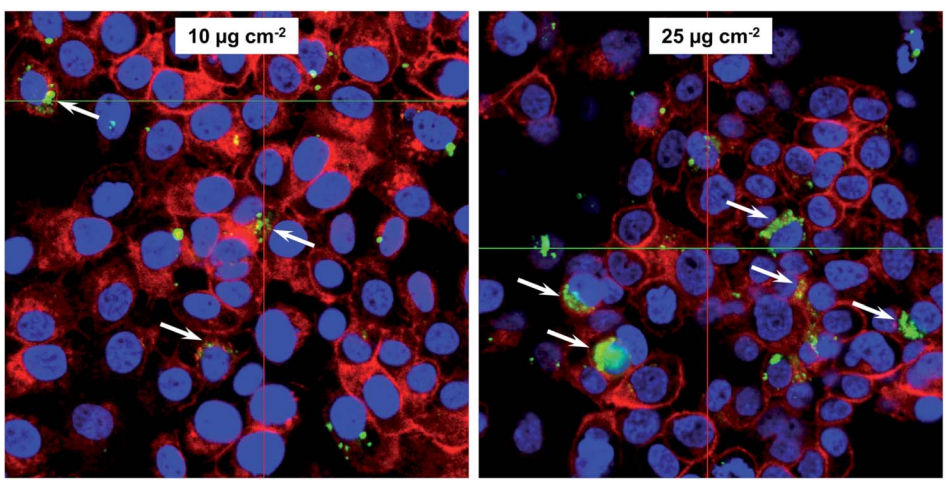

Fig. 4 Internalization of magnetosomes by FaDu cells. Confocal laser scanning microscopy (cLSM) analysis of FaDu cells incubated with fluorescent, DyLight488-labelled WT magnetosomes (10 or 25 μg Fe cm^{-2}) for 24 h. cLSM indicated that the particles are taken up by the cells and localize in endolysosomes around the nucleus (white arrows). Fluorescent magnetosomes, green; actin cytoskeleton (phalloidin-AF633), red; nuclei (hoechst33258), blue.

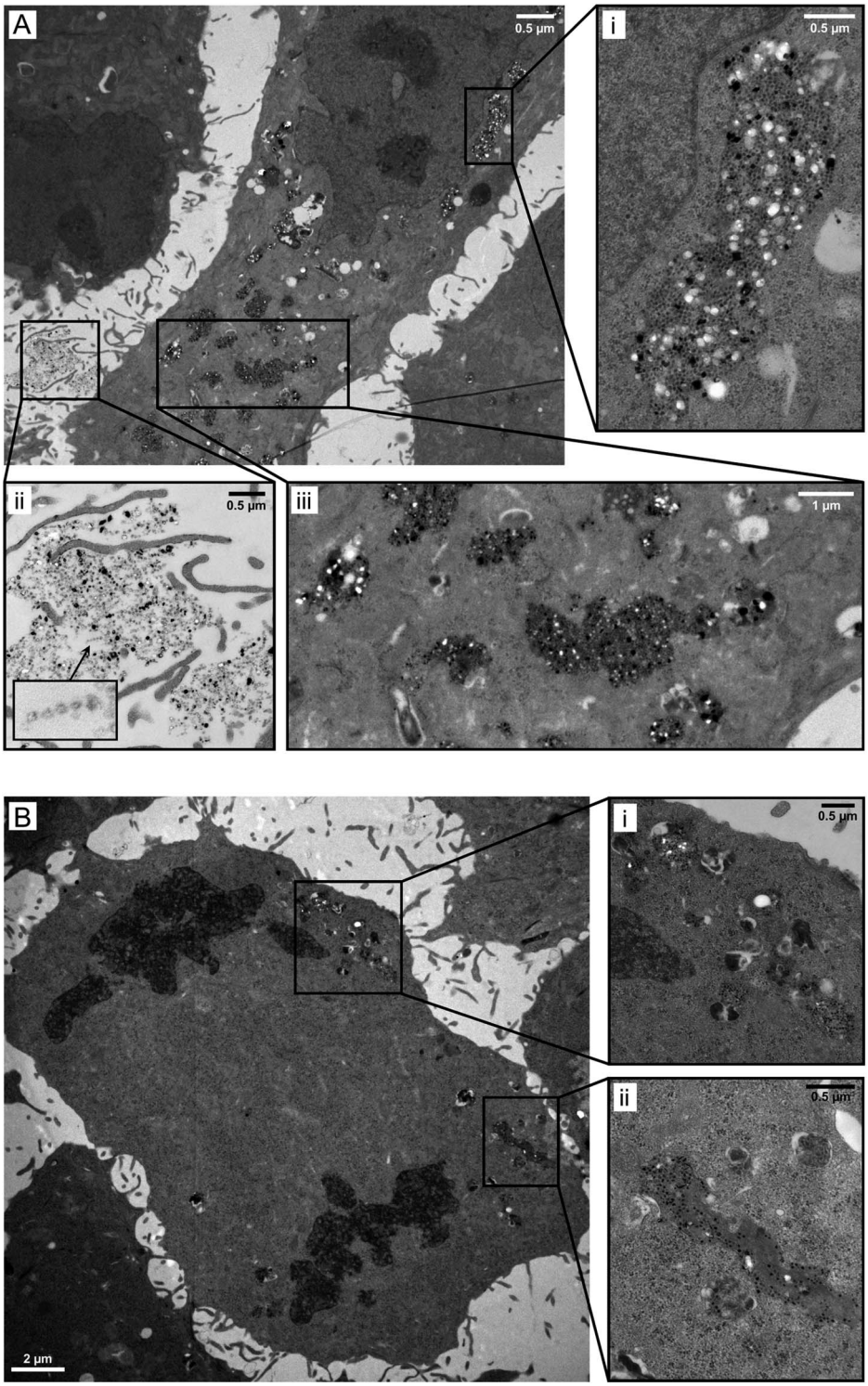

Fig. 5 Magnetosome uptake by FaDu cells and subcellular localization. FaDu cells were grown on coverslips and incubated with WT magnetosomes. After fixation, dehydration and flat embedding, ultrathin serial sections were cut and screened for particle internalization using transmission electron microscopy. (A) TEM micrographs of ultrathin sections demonstrate magnetosome uptake, which is indicated by high amounts of electron-dense particles being internalized in vesicle-like structures (iii), partially located in close proximity to the nucleus (i). In addition to magnetosomes taken up by the cells, well-dispersed particles can be found in the area surrounding the cells (ii), forming the typical chain-like arrangements (inset). (B) TEM image of a representative dividing FaDu cell, showing internalized magnetosomes. Even for dividing cells, vesicle-like structures could be found, filled with high amounts of electron-dense nanoparticles (shown in more detail in the magnifications (i) and (ii)).

on the proliferation behavior, transduced FaDu cells with red-fluorescent nuclei (FaDu-NR) were incubated with different particle amounts ranging from 5 to 100 μg cm^{-2} for 44 h. IncuCyte real-time analyses on the cellular growth revealed concentration-dependent effects on the proliferation rates (Fig. 6). For a magnetosome concentration of 5 μg cm^{-2} growth was comparable to that of untreated FaDu-NR cells or cells that were incubated with HEPES buffer, with doubling times of ~28 h. Increasing magnetosome amounts significantly reduced cellular growth. Thus, at 25 μg cm^{-2} a doubling time of ~45 h was measured, and at 50 and 100 μg cm^{-2} cellular growth was completely inhibited. However, microscopy analysis (Fig. S6†) clearly indicated the presence of intact cells that were just "trapped" and thus, unable to proliferate. These observations are in agreement with the described viability assays (Fig. 2 and 3). In contrast, treatment with Triton X-100 or PEI-coated nanoparticles (50 μg cm^{-2}) drastically reduced FaDu-NR fluorescence below the initial value at t_0. Here, after 8 h of incubation, a dramatic loss of the fluorescence signal was observed, indicating cell death.

As increasing particle amounts (25–100 μg cm^{-2}) affected proliferation of the FaDu-NR cells, we asked whether the presence of the applied magnetosome amounts throughout the analysis or the magnetosomes attached to the cell surface and the incorporated particles are responsible for that observation. To prove this hypothesis, FaDu-NR cells were incubated with 25 μg cm^{-2} magnetosomes for 24 h. Afterwards, the cell suspension was concentrated and magnetically enriched, and defined numbers of cells were seeded into fresh medium. The time-dependent cell proliferation was monitored for 102 h (Fig. 7A), and growth rates gradually increased with the number of FaDu cells seeded (proliferation is given as "confluency of cell layer [%]", directly correlating with the cellular growth). The 200 K fraction and the 100 K fraction reached confluency after 72 h and 102 h, respectively. The calculated doubling time for these fractions is 22 to 26 h, whereas for the 50 K fraction is approximately 30 h. This is in good accordance to the specification of the DSMZ. Moreover, for the respective cell numbers of both the untreated FaDu cells ("Control") and cells incubated in the presence of magnetosomes ("Magnetos.") a nearly identical growth behavior was detected. These observations suggest that magnetosome treatment only reversibly inhibited cell proliferation. The separation of the magnetosome-treated cells *via* MACS even enriched the vital cells. Thus, after dissemination and consequent reduction of the magnetosome load by dilution, the cells continued proliferating.

In order to investigate further effects of magnetosome-treatment and magnetic separation, we subjected 150 000 FaDu cells to MACS MS columns after incubation with 25 μg cm^{-2} magnetosomes. After elution/passing the magnetic column, the proliferation behavior of the respective fractions was analyzed (Fig. 7B). Thereby, untreated FaDu cells ("w/o magnetosomes, w/o magnetic separation") and the magnetosome-incubated cells that were magnetically retained in the column ("positive fraction") exhibited comparable growth rates. It should be considered that in the course of magnetic separation, the majority of the magnetosome-incubated cells could be retained within the column, and only

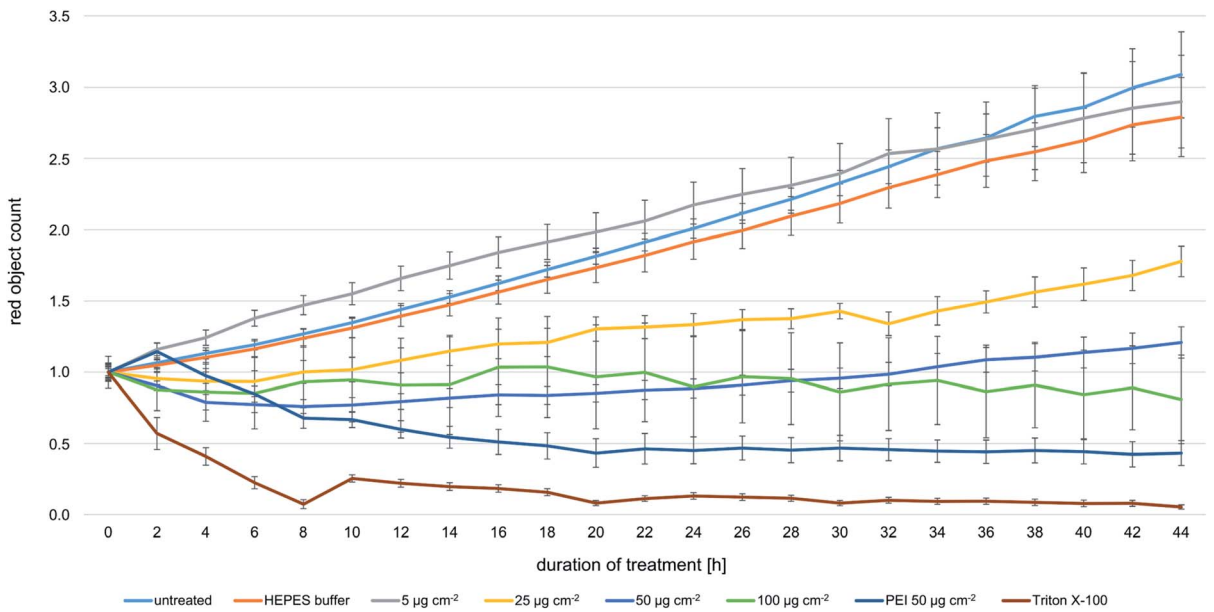

Fig. 6 Real-time analysis of the proliferation behavior of magnetosome-treated FaDu-NR cells. In order to investigate potential effects on cellular growth, transduced FaDu-NR cells were incubated with the indicated magnetosome concentrations, ranging from 5 to 100 μg cm^{-2}. The IncuCyte ZOOM system was used to determine the number of red-fluorescent nuclei (denominated as "red object count") as a measure for the number of vital cells. Untreated FaDu-NR cells and cells incubated with HEPES buffer served as positive control, cells treated with 0.1% Triton X-100 or PEI-coated nanoparticles (50 μg cm^{-2}) were used as negative control, as incubation with the FaDu-NR cells led to cell death. For the magnetosome-treated fractions, a concentration-dependent decrease of the fluorescence signal was observed, indicating impaired proliferation. Number of biological replicates: $n = 3$, each measured in quadruplicates.

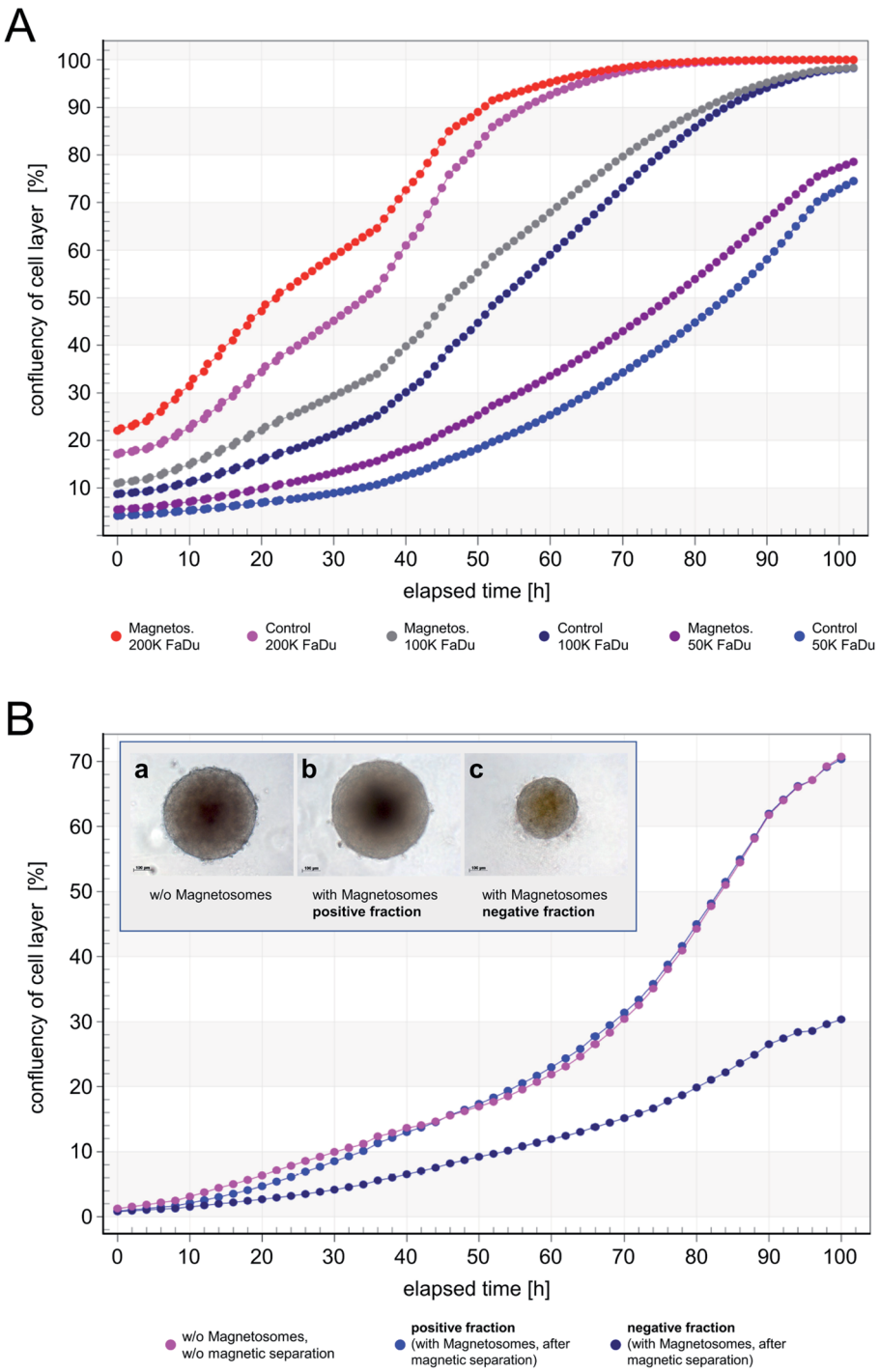

Fig. 7 Cellular growth and spheroid formation of FaDu-NR cells after magnetosome loading. (A) FaDu-NR cells were incubated with 25 μg cm^{-2} magnetosomes for 24 h. After magnetic enrichment by subjecting the mixture to MACS MS columns, the indicated, defined cell numbers were seeded into fresh medium to allow for proliferation. The time-dependent cellular growth was monitored for 102 h ("Magnetos.") and compared to the untreated cell fractions ("Control"). For both, the untreated and the corresponding positive fractions, nearly identical growth patterns were observed, and proliferation rates gradually increased with the number of FaDu-NR cells seeded. Proliferation is given as "confluency of cell layer [%]", directly correlating with the cellular growth. (B) 150 000 FaDu-NR cells were subjected to magnetic separation after incubation with 25 μg cm^{-2} magnetosomes. The majority of the magnetosome-treated FaDu-NR cells was retained in the matrix and only eluted after removal of the magnetic field ("positive fraction"). Afterwards, the cellular growth was analyzed, which was comparable to untreated FaDu-NR cells ("w/o magnetosomes, w/o magnetic separation"). Only a low number of magnetosome-treated FaDu-NR cells was directly eluted from the column ("negative fraction"). Therefore, due to the reduced number of cells in the proliferation assay, decreased growth rates (compared to those of the "positive fraction") were observed. As a further proof of adequate cell behavior, the formation of spheroids was analyzed. For that purpose, FaDu-NR cells were seeded in u-bottom shaped 96-well plates and monitored in the IncuCyte system for 96 h. Inset: (a) FaDu-NR cells without magnetosome-incubation, without magnetic separation (5000 cells seeded); (b) FaDu-NR cells with magnetosome-incubation, magnetic separation – positive fraction (5000 cells seeded); (c) FaDu-NR cells with magnetosome-incubation, magnetic separation – negative fraction (2000 cells seeded).

a low number of cells was directly eluted. Therefore, due to this reduced number of cells in the "negative fraction", the respective proliferation curve was clearly below that of the "positive fraction".

In addition, the formation of spheroids as an indicator for adequate cell behavior was investigated. The interaction of cells is inevitable to form structures that are more complex. A common lab model for interaction is the formation of 3-dimensional cell aggregates known as multicellular spheroids. Cells within these structures form an extracellular matrix and are polarized. As shown in Fig. 7B (insets) and S7,† in the presence of magnetosomes the ability to form well-shaped spheroids was not affected, indicating that the overall cell behavior is not impaired.

Short-term labelling of FaDu cells with magnetosomes enables cellular magnetization

Next, we compared magnetosomes–FaDu and magnetosomes–leukocytes interactions upon short-term incubation. For that purpose, we incubated 1×10^6 FaDu-NR cells or 2.5×10^6 leukocytes with unlabelled magnetosomes (10–100 μg Fe mL^{-1}) for 8 min. The suspensions were subsequently subjected to magnetic columns that allow for magnetic separation of particle-labelled/loaded cells. Both, cells of the flow-through (*i.e.* the negative fraction) and cells that were retained in the magnetic field (*i.e.* the positive fraction) were counted (Fig. 8A).

For all tested particle concentrations, only low numbers of leukocytes were sufficiently loaded to be retained by the magnetic field (less than 10% of the total cell number), indicating weak interactions with magnetosomes. FaDu-NR cells, in contrast, exhibited significantly increased retention rates. Thus, already for magnetosome amounts corresponding to 10 μg Fe mL^{-1} more than 35% of the total cell number could be magnetically separated. The latter could be further increased by incubation with higher particle amounts, with 25, 50 and 100 μg Fe mL^{-1} retaining more than 50–60% of the cells. Thereby, for iron concentration ≥25 μg mL^{-1}, similarly 'magnetized' FaDu-NR cell numbers were counted, suggesting an upcoming saturation effect. In order to roughly simulate a composition/configuration theoretically found in peripheral blood samples, we mixed low amounts of FaDu-NR cells (125 000; 5% of the total cell number) with a high portion of leukocytes (2.5×10^6; corresponding to 95% of the total cell amount), and incubated the cell suspension with magnetosomes (25 μg Fe mL^{-1}) (Fig. 8B). After magnetic sorting, the overall number of cells retained in the magnetic field was less than 5%; however, with incremental incubation times, an increased portion of FaDu-NR cells could be magnetically separated (>30% of the total FaDu-NR cell number after an incubation time of 20 min). Similar observations had been made before for leukocyte/breast cancer cell mixtures incubated with carboxymethyl-dextran coated iron oxide nanoparticles,[55,56] and might be explained by a more

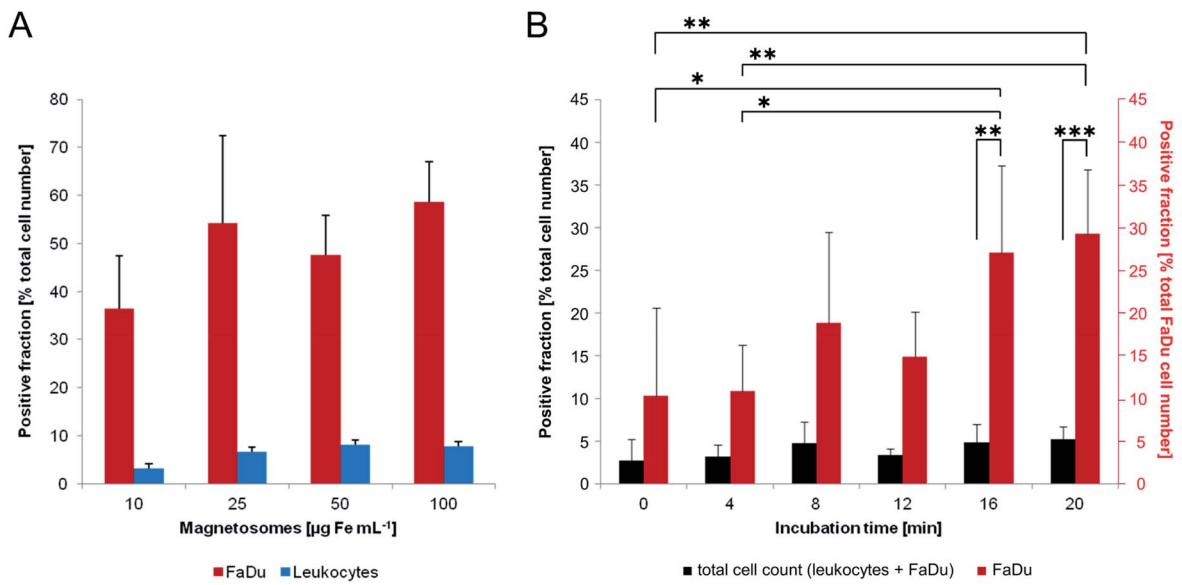

Fig. 8 Interaction of magnetosomes with FaDu-NR cells and magnetic separation of particle-loaded cells. (A) 1×10^6 FaDu-NR cells or 2.5×10^6 leukocytes were incubated with magnetosomes (10–100 μg mL^{-1}) for 8 min. The suspensions were subsequently separated using magnetic columns, and cells of the flow-through (negative fraction) and cells retained in the magnetic field (positive fraction) were counted. Whereas for the leukocytes only weak interactions were detected (most cells were found in the flow-through), up to 60% of the FaDu-NR cells could be retained in the columns, indicating a sufficient particle-labelling for magnetic separation. Cell loss: 2–20%, $n = 2$. (B) 125 000 FaDu-NR cells were mixed with 2.5×10^6 leukocytes and subsequently treated with magnetosomes (25 μg Fe mL^{-1}) for different incubation times (up to 20 min). As described in (A), the suspensions were magnetically separated and cells of the positive and negative fraction were counted. Flow cytometry was used to determine the portion of FaDu-NR cells. With increasing incubation times, a significant increase of the portion of particle-labelled FaDu-NR cells was observed in the positive fraction, whereas the total cell number stayed constant in the range from 2–5%. These finding argue for increased interaction of magnetosomes with the tumor cell line (compared to leukocytes). Cell loss <15%, $n = 4$. Statistically significant differences are denoted as follows: $p < 0.05$ (*), $p < 0.01$ (**), $p < 0.001$ (***).

negative net surface charge and a higher membrane turnover of the cancer cells compared to primary cells.[57,58] Thus, in the investigated leukocyte/FaDu-NR mixture, magnetosome–cell interactions seemed to be increased for the FaDu cancer cell line (compared to the leukocytes). The treatment with magnetosomes might therefore be used to efficiently magnetize and consequently magnetically enrich tumor cells from cell mixtures.

Discussion

In our study, we in-depth assessed the biocompatibility of isolated magnetosomes, as well as particle–cell interactions upon magnetosome-treatment of different mammalian cell lines. As the uptake of individual particles or smaller chains is presumably favored compared to particle agglomerates, we first investigated the stability of magnetosome suspensions in physiological fluids, thereby mimicking conditions found *in vivo*. Different particle concentrations were incubated in complex cell culture media that might lead to particle agglomeration or even compromise the surrounding magnetosome membrane. Our data suggest the co-existence of different species, which could be explained by the formation of smaller agglomerates, chains or combinations thereof. The tendency of isolated magnetosomes to form chain-like structures and agglomerates has been reported before.[29,59] Magnetic attraction as well as the particle surface charge (*i.e.* the charge patches of the proteins and lipid compounds of the magnetosome membrane) and Van-der-Waals forces are supposed to influence particle–particle interactions. Furthermore, the concentration of FBS in the culture media seems to influence the agglomeration tendencies. Thus, with increasing FBS contents, a trend towards smaller aggregates or individually dispersed particles was observed. These findings might be explained by the formation of a protein corona on the magnetosome surface that could have reduced particle–particle interactions. The formation of such a shell has been investigated before. For instance, Gräfe and co-workers[43] incubated PEI-coated magnetic nanoparticles in different FBS concentrations, and the amount of corona proteins bound to the particle surface was increased with the FBS content, thereby "shielding" the particles and even reducing the interaction with HBMEC.

Moreover, the sizes of agglomerates or particle chains increased with prolonged incubation times (up to 48 h), however, the obtained values (<800 nm) still suggested a general suitability for the uptake by mammalian cells,[6] which might represent a prerequisite for further investigations on biocompatibility and magnetosome–cell interactions.

So far, the cytotoxicity of bacterial magnetosomes has been investigated on several diverse mammalian cell lines; usually particle amounts in the range from 10 μg to 1.0 mg are applied. However, obtained values often significantly differ depending on the tested cell line. For instance, for H22 mouse hepatoma cells or the HL60 human peripheral blood cell line a particle concentration of 9 μg mL^{-1} was sufficient to cause cytotoxic effects.[60] In the same study, Sun and co-workers also performed investigations on EMT-6 and MDA-MB-231 cells, and for particle amounts ≥1.0 mg no or only low cytotoxic effects were observed. In a related study, Mannucci *et al.* evaluated potential cytotoxic effects of magnetosomes isolated from *M. gryphiswaldense* on HT-29 (human colon carcinoma) and U87MG (human glioblastoma-astrocytoma, epithelial-like) cells.[24] In MTT assays, only moderate through negligible effects on cell viability were observed when treated with particle concentrations of 0.2, 0.5 or 1.0 mg mL^{-1}. Similar observations were made for ARPE-19 cells (adult retinal pigment epithelial cell line-19) incubated with particle amounts corresponding to 10, 50 or 100 μg Fe mL^{-1}. Here, assays were applied that detected the cell membrane integrity (LDH assay) or the activity of intracellular dehydrogenases (CCK-8 assay). After 72 h of incubation, even for the highest tested particle concentration (100 μg mL^{-1}) cell viability was only slightly reduced, with values >90%. Furthermore, the survival rates of ARPE-19 cells decreased with increasing magnetosome concentrations and incubation times. After 48 h incubation at 100 μg mL^{-1}, a cell survival rate of approximately 65% was determined.[60,61]

In our study, viability values obtained for magnetosome treatment of up to 24 h indicated a robust biocompatibility for particle concentrations ranging from 5–100 μg cm^{-2} (which roughly equals 20–400 μg mL^{-1}) (Fig. 2). Thereby, as expected the treated cell lines (BeWo, FaDu, HCC78 and hPC-PL) differed in their sensitivity; however, for HCC78 cells which exhibited the strongest decrease in viability still values >70% were observed. Extended incubation times up to 48 h further reduced cell viability rates, and for all tested cell lines trends towards decreasing viability values were observed. Overall, as observed in our previous study,[29] the FaDu cell line turned out to be more robust, and even for 100 μg Fe cm^{-2} and 48 h of incubation values >90% were measured. BeWo, hPC-PL and in particular HCC78 seemed to be more sensitive to magnetosome treatment, and after 48 h viability partially dropped to 50–70%. Although under these conditions the value classified as moderate cell viability (≥69%; EN ISO 10993-5:2009)[48] could not be reached, for many envisioned *in vivo* applications *e.g.* as contrast agents[26,28,62] or for magnetic hyperthermia[23,63,64] the retention time within the body is usually quite low, and the particles are removed from the blood stream and excreted/degraded after several hours.[5,6] The provided biocompatibility for 24 h of incubation might therefore provide a general suitability of magnetosomes not only for diagnostic, but also for potential *in vivo* applications.

Further analyses regarding the fate of the particles upon (prolonged) incubation were performed on the FaDu cell line. TEM and cLSM clearly revealed magnetosome uptake and accumulation within the cells (Fig. 4 and 5). Thereby, typical endolysosomal signatures were observed, with high particle amounts being internalized in vesicle-like structures in the cytoplasm and partially in direct vicinity to the nuclei, indicating endocytic uptake as it has also been suggested for other cell lines. For instance, after incubation of HeLa cells with various amounts of magnetosomes isolated from *Magnetovibrio blakemorei* MV-1 or *M. magneticum* AMB-1 for 12–24 h,[65,66] particle internalization into endosomal or lysosomal vesicles was observed. Similarly, Wang *et al.*[67] investigated the

interaction and uptake of magnetosomes (from *M. magneticum* AMB-1) by human hepatoblastoma (HepG2) cells. As for the HeLa cells, particles could bind to the cell surface and accumulated in endosomes and lysosomes in a concentration-dependent manner. In a related study, Mannucci and co-workers[68] studied the uptake of magnetosomes isolated from *M. gryphiswaldense*. The authors exposed U87MG cells to varying particle concentrations, and magnetosome amounts of 0.2 mg mL^{-1} and an incubation time of 24 h were suggested as best conditions for internalization. Thereby, particles were distributed on the cellular membrane, within cytoplasmic vacuoles and near the nucleus.

Upon long-term magnetosome-treatment, a concentration-dependent effect on the proliferation of FaDu cells was observed, with a particle amount $\geq$50 μg cm^{-2} repressing cell growth dramatically. Interestingly, after magnetic separation of magnetosome-treated FaDu cells and further reduction of the particle concentration in the surrounding medium by dissemination of the cells, growth rates comparable to untreated FaDu cell cultures could be recovered. As observed for chemically synthesized/artificial iron oxide nanoparticles,[43,69,70] components of the cell culture medium (such as proteins of the FBS) might unspecifically bind to the magnetosome surface, resulting in a corona of a variety of biomolecules on the magnetosome membrane. As the latter is associated with a high number of integral proteins (tightly packed within the phospholipid bilayer) as well as proteins electrostatically bound to the surface,[13,14] the formation of a complex biomolecule "network" could be hypothesized, that might crucially reduce the amount of available nutrients and trace elements in the medium. Moreover, the presence of increased particle amounts in direct vicinity to the cells could disturb redox states and/or cause local pH shifts. The evaluation of such "stress factors" will be subject of future studies, however, it can be assumed that magnetosome treatment impairs cell culture conditions and in consequence pause cell proliferation. In contrast, particle internalization into magnetosome-filled vesicles did not seem to affect proliferation of the cells. This is also obvious from TEM analyses, which confirmed the presence of internalized magnetosomes in dividing cells (Fig. 5B). Furthermore, magnetosome-treated cells were shown to form three-dimensional cell cultures (spheroids), indicating cell integrity with regard to cell migration, differentiation capabilities and growth.[71] These findings are in accordance with observations made, for instance, by Curcio *et al.*[72] In the latter study, the uptake of magnetosomes isolated from *M. magneticum* AMB-1 by human stem cells and particle degradation have been investigated. Thereby, magnetosome internalization did not affect cellular growth, which could be demonstrated by the formation of spheroids. A distinct (narrow) particle size range was found to be favored for uptake, and cells could be efficiently magnetized exhibiting ferromagnetic characteristics.

When applying magnetosomes at different amounts to FaDu cells, we could demonstrate that even short-term incubation is sufficient to efficiently magnetize the cells. Thus, up to 60% of the magnetosome-treated FaDu cells could be magnetically separated after 8 min of incubation. A combination of unspecific interactions with the FaDu cell surface and particle internalization might together contribute to cell magnetization. Furthermore, magnetosomes preferentially interacted with the cancer cell line compared to leukocytes and were taken up at elevated rates. The efficient particle uptake and high cell viability rates could therefore be of great importance for the future use of bacterial magnetosomes as *e.g.* targeting agents for cancer cells, in particular circulating tumor cells (CTCs).[30,73]

Conclusions and outlook

In our study, we provide a comprehensive assessment of the biocompatibility of bacterial magnetosomes on the cell culture level, including different cancer cell lines and more sensitive primary cells. Different parameters are critically evaluated, including viability (*i.e.* the metabolic activity of the cells), cell death events in the course of magnetosome treatment as well as potential effects on proliferation. The data obtained from different assays performed are finally combined to an overall picture. Across the different tested cell lines, viability was only slightly affected, even for increased magnetosome concentrations. Our data therefore suggest that magnetosomes might be well-suited for applications in the field of diagnostics. However, for future *in vivo* applications further toxicity factors such as antigenicity and endotoxicity still have to be evaluated due to the bacterial origin of the particles.[74] Overcoming these limitations (*e.g.* by camouflaging the particle surface with biocompatible coatings) might turn bacterial magnetosomes a promising alternative to chemically synthesized nanoparticle formulations. Thereby, future *in vivo* applications might benefit from the feasibility to genetically engineer the enveloping magnetosome membrane.[75,76] In particular the magnetosome display of antibodies, specific ligands or recognition elements for tumor cells might provide a promising route for cancer cell targeting by enhanced magnetosome–cell interactions. The feasibility of such an approach has been demonstrated by decorating isolated magnetosomes with specialized targeting peptides such as P75 (specific for EGFR and HER2),[77] pHLIP (pH low insertion peptide)[78] or RGD (integrin-binding peptide).[78,79] In all cases, the functionalized magnetosomes showed specific, increased binding to selected cancer cell lines (displaying the corresponding interaction partners) and accumulation at the tumor site, thereby significantly enhancing the tumor contrast on MR images. Thus, isolated (functionalized) magnetosomes could serve as a theranostic tool for many future applications in the (bio)medical field, combining diagnostic and therapeutic functions at the same time.

Conflicts of interest

There are no conflicts to declare.

Acknowledgements

The authors are grateful to Matthias Schlotter (Dept. Microbiology, University of Bayreuth) for technical assistance with cell cultivation, magnetosome isolation and iron measurements. Rita

Grotjahn (Electron microscopy, University of Bayreuth) is acknowledged for technical assistance with transmission electron microscopy. This project was funded in part from the Deutsche Forschungsgemeinschaft (DFG), grant CL-202/3-3 (JC). Further funding was received from the European Research Council (ERC) under the European Union's Horizon 2020 research and innovation program (grant agreement No. 692637 to DS), and the Federal Ministry of Education and Research (BMBF) (grant MagBioFab to DS). In addition, this work was supported in part by Europäische Fonds für regionale Entwicklung-Europa für Thüringen (EFRE, FKZ 2016 FGI 0006) (JC).

Notes and references

1 J. B. Haun, T. J. Yoon, H. Lee and R. Weissleder, *Wiley Interdiscip. Rev.: Nanomed. Nanobiotechnol.*, 2010, **2**, 291–304.
2 M. Hepel, *Magnetochemistry*, 2020, **6**, 3.
3 C. Sun, J. S. Lee and M. Zhang, *Adv. Drug Delivery Rev.*, 2008, **60**, 1252–1265.
4 J. R. McCarthy and R. Weissleder, *Adv. Drug Delivery Rev.*, 2008, **60**, 1241–1251.
5 C. C. Berry and A. S. Curtis, *J. Phys. D: Appl. Phys.*, 2003, **36**, R198.
6 K. El-Boubbou, *Nanomedicine*, 2018, **13**, 953–971.
7 J. Mosayebi, M. Kiyasatfar and S. Laurent, *Adv. Healthcare Mater.*, 2017, **6**, 1700306.
8 A. S. Teja and P. Y. Koh, *Prog. Cryst. Growth Charact. Mater.*, 2009, **55**, 22–45.
9 M. R. Zamani Kouhpanji and B. J. Stadler, *Sensors*, 2020, **20**, 2554.
10 C. Jogler and D. Schüler, *Annu. Rev. Microbiol.*, 2009, **63**, 501–521.
11 R. Uebe and D. Schüler, *Nat. Rev. Microbiol.*, 2016, **14**, 621–637.
12 K. Grünberg, C. Wawer, B. M. Tebo and D. Schüler, *Appl. Environ. Microbiol.*, 2011, **67**, 4573–4582.
13 K. Grünberg, E.-C. Müller, A. Otto, R. Reszka, D. Linder, M. Kube, R. Reinhardt and D. Schüler, *Appl. Environ. Microbiol.*, 2004, **70**, 1040–1050.
14 O. Raschdorf, F. Bonn, N. Zeytuni, R. Zarivach, D. Becher and D. Schüler, *J. Proteomics*, 2018, **172**, 89–99.
15 S. S. Staniland, B. Ward, A. Harrison, G. van der Laan and N. Telling, *Proc. Natl. Acad. Sci. U. S. A.*, 2007, **104**, 19524–19528.
16 S. S. Staniland and A. E. Rawlings, *Biochem. Soc. Trans.*, 2016, **44**, 883–890.
17 D. Faivre and D. Schüler, *Chem. Rev.*, 2008, **108**, 4875–4898.
18 E. Alphandéry, *Front. Bioeng. Biotechnol.*, 2014, **2**, 5.
19 L. Yan, H. Da, S. Zhang, V. M. López and W. Wang, *Microbiol. Res.*, 2017, **203**, 19–28.
20 G. Vargas, J. Cypriano, T. Correa, P. Leão, D. A. Bazylinski and F. Abreu, *Molecules*, 2018, **23**, 2438.
21 E. Alphandéry, F. Guyot and I. Chebbi, *Int. J. Pharm.*, 2012, **434**, 444–452.
22 R. Weissleder, A. Moore, U. Mahmood, R. Bhorade, H. Benveniste, E. A. Chiocca and J. P. Basilion, *Nat. Med.*, 2000, **6**, 351–354.
23 R. T. Liu, J. Liu, J. Q. Tong, T. Tang, W. C. Kong, X. W. Wang, Y. Li and J. T. Tang, *Prog. Nat. Sci.: Mater. Int.*, 2012, **22**, 31–39.
24 S. Mannucci, L. Ghin, G. Conti, S. Tambalo, A. Lascialfari, T. Orlando, D. Benati, P. Bernardi, N. Betterle, R. Bassi, P. Marzola and A. Sbarbati, *PLoS One*, 2014, **9**, e108959.
25 M. L. Fdez-Gubieda, J. Alonso, A. García-Prieto, A. García-Arribas, L. Fernández Barquín and A. Muela, *J. Appl. Phys.*, 2020, **128**, 070902.
26 R. Taukulis, M. Widdrat, M. Kumari, D. Heinke, M. Rumpler, É. Tompa, R. Uebe, A. Kraupner, A. Cebers, D. Schüler, M. Pósfai, A. M. Hirt and D. Faivre, *Magnetohydrodynamics*, 2015, **51**, 721–747.
27 D. Heinke, A. Kraupner, D. Eberbeck, D. Schmidt, P. Radon, R. Uebe, D. Schüler and A. Briel, *Int. J. Mag. Part. Imag.*, 2017, **3**, 1706004.
28 T. Orlando, S. Mannucci, E. Fantechi, G. Conti, S. Tambalo, A. Busato, C. Innocenti, L. Ghin, R. Bassi, P. Arosio, F. Orsini, C. Sangregorio, M. Corti, M. F. Casula, P. Marzola, A. Lascialfari and A. Sbarbati, *Contrast Media Mol. Imaging*, 2016, **11**, 139–145.
29 S. Rosenfeldt, F. Mickoleit, C. Jörke, J. H. Clement, S. Markert, V. Jérôme, S. Schwarzinger, R. Freitag, D. Schüler, R. Uebe and A. S. Schenk, *Acta Biomater.*, 2021, **120**, 293–303.
30 N. Hao and J. X. Zhang, *Biomicrofluidics*, 2019, **13**, 051501.
31 S. R. S. Rangan, *Cancer*, 1972, **29**, 117–121.
32 A. K. Virmani, K. M. Fong, D. Kodagoda, D. McIntire, J. Hung, V. Tonk, J. D. Minna and A. F. Gazdar, *Genes, Chromosomes Cancer*, 1998, **21**, 308–319.
33 R. A. Pattillo and G. O. Gey, *Cancer Res.*, 1968, **28**, 1231–1236.
34 D. Schultheiss and D. Schüler, *Arch. Microbiol.*, 2003, **179**, 89–94.
35 U. Heyen and D. Schüler, *Appl. Microbiol. Biotechnol.*, 2003, **61**, 536–544.
36 C. Lang and D. Schüler, *Appl. Environ. Microbiol.*, 2008, **74**, 4944–4953.
37 S. Geimer, *Methods Cell Biol.*, 2009, **91**, 63–80.
38 E. S. Reynolds, *J. Cell Biol.*, 1963, **17**, 208–212.
39 T. Schlorf, M. Meincke, E. Kossel, C. C. Gluer, O. Jansen and R. Mentlein, *Int. J. Mol. Sci.*, 2011, **12**, 12–23.
40 F. Bähring, F. Schlenk, J. Wotschadlo, N. Buske, T. Liebert, C. Bergemann, T. Heinze, A. Hochhaus, D. Fischer and J. H. Clement, *IEEE Trans. Magn.*, 2013, **49**, 383–388.
41 A. Theumer, C. Gräfe, F. Bähring, C. Bergemann, A. Hochhaus and J. H. Clement, *J. Magn. Magn. Mater.*, 2015, **380**, 27–33.
42 J. W. Tukey, *Biometrics*, 1949, **5**, 99–114.
43 C. Gräfe, A. Weidner, M. v. d. Lühe, C. Bergemann, F. H. Schacher, J. H. Clement and S. Dutz, *Int. J. Biochem. Cell Biol.*, 2016, **75**, 196–202.
44 T. Cedervall, I. Lynch, S. Lindman, T. Berggård, E. Thulin, H. Nilsson, K. A. Dawson and S. Linse, *Proc. Natl. Acad. Sci. U. S. A.*, 2007, **104**, 2050–2055.
45 M. Lundqvist, J. Stigler, G. Elia, I. Lynch, T. Cedervall and K. A. Dawson, *Proc. Natl. Acad. Sci. U. S. A.*, 2008, **105**, 14265–14270.

46 G. Maiorano, S. Sabella, B. Sorce, V. Brunetti, M. A. Malvindi, R. Cingolani and P. P. Pompa, *ACS Nano*, 2010, **4**, 7481–7491.
47 T. Ackermann and S. Tardito, *Trends Cancer*, 2019, **5**, 329–332.
48 DIN Deutsches Institut für Normen e.V. Biologische Beurteilung von Medizinprodukten – Teil 5: Prüfungen auf *in vitro*-Zytotoxizität (ISO 10993-5:2009); Deutsche Fassung EN ISO 10993-5:2009, 2009.
49 R. I. Freshney, *Culture of animal cells. A manual of basic technique*, Wiley-Liss, Inc., 605 Third Avenue, New York, NY, USA, 2nd edn, 1987, p. 68ff.
50 K. Xiong, W. Wie, Y. Jin, S. Wang, D. Zhao, S. Wang, X. Gao, C. Qiao, H. Yue, G. Ma and H. Y. Xie, *Adv. Mater.*, 2016, **28**, 7929–7935.
51 C. Alix-Panabieres and K. Pantel, *Nat. Rev. Cancer*, 2014, **14**, 623–631.
52 C. Y. Wen, L. L. Wu, Z. L. Zhang, Y. L. Liu, S. Z. Wei, J. Hu, M. Tang, E. Z. Sun, Y. P. Gong, J. Yu and D. W. Pang, *ACS Nano*, 2014, **8**, 941–949.
53 U. Termsarasab, H. J. Cho, H. T. Moon, J. H. Park, I. S. Yoon and D. D. Kim, *Colloids Surf., B*, 2013, **109**, 280–286.
54 B. Fahmy and S. A. Cormier, *Toxicol. In Vitro*, 2009, **23**, 1365–1371.
55 J. H. Clement, M. Schwalbe, N. Buske, K. Wagner, M. Schnabelrauch, P. Görnert, K. O. Kliche, K. Pachmann, W. Weitschies and K. Höffken, *J. Cancer Res. Clin. Oncol.*, 2006, **132**, 287–292.
56 M. Schwalbe, K. Pachmann, K. Höffken and J. H. Clement, *J. Phys.: Condens. Matter*, 2006, **18**, 2865–2876.
57 B. Alberts, A. Johnson, J. Lewis, M. Raff, K. Roberts and P. Walter, *Molecular Biology of the Cell*, Garland Science, New York, 4th edn, ch. 13, 2002, pp. 739–756.
58 K. M. Yamada, S. H. Ohanian and I. Pastan, *Cell*, 1976, **9**, 241–245.
59 A. P. Philipse and D. Maas, *Langmuir*, 2002, **18**, 9977–9984.
60 J. B. Sun, T. Tang, J. Duan, P. Xu, Z. Wang, Y. Zhang, L. Wu and Y. Li, *Nanotoxicol*, 2010, **4**, 271–283.
61 L. Qi, X. Lv, T. Zhang, P. Jia, R. Yan, S. Li, R. Zou, Y. Xue and L. Dai, *Sci. Rep.*, 2016, **6**, 26961.
62 A. Kraupner, D. Eberbeck, D. Heinke, R. Uebe, D. Schüler and A. Briel, *Nanoscale*, 2017, **9**, 5788–5793.
63 R. Hergt, R. Hiergeist, M. Zeisberger, D. Schüler, U. Heyen, I. Hilger and W. A. Kaiser, *J. Magn. Magn. Mater.*, 2005, **293**, 80–86.
64 E. Alphandéry, S. Faure, O. Seksek, F. Guyot and I. Chebbi, *ACS Nano*, 2011, **5**, 6279–6296.
65 J. Cypriano, J. Werckmann, G. Vargas, A. Lopes dos Santos, K. T. Silva, P. Leão, F. P. Almeida, D. A. Bazylinski, M. Farina, U. Lins and F. Abreu, *PLoS One*, 2019, **14**, e0215657.
66 J. Shin, C. H. Yoo, J. Lee and M. Cha, *Biomaterials*, 2012, **33**, 5650–5657.
67 P. Wang, C. Chen, C. Chen, Y. Li, W. Pan and T. Song, *J. Magn. Magn. Mater.*, 2017, **427**, 105–110.
68 S. Mannucci, S. Tambalo, G. Conti, L. Ghin, A. Milanese, A. Carboncino, E. Nicolato, M. R. Marinozzi, D. Benati, R. Bassi, P. Marzola and A. Sbarbati, *Contrast Media Mol. Imaging*, 2018, 2198703.
69 M. M. Yallapu, N. Chauhan, S. F. Othman, V. Khalilzad-Sharghi, M. C. Ebeling, S. Khan, M. Jaggi and S. C. Chauhan, *Biomaterials*, 2015, **46**, 1–12.
70 A. Weidner, C. Gräfe, M. v. d. Lühe, H. Remmer, J. H. Clement, D. Eberbeck, F. Ludwig, R. Müller, F. H. Schacher and S. Dutz, *Nanoscale Res. Lett.*, 2015, **10**, 282.
71 L. Griffith and M. Swartz, *Nat. Rev. Mol. Cell Biol.*, 2006, **7**, 211–224.
72 A. Curcio, A. Van de Walle, A. Serrano, S. Preveral, C. Péchoux, D. Pignol, N. Menguy, C. T. Lefevre, A. Espinosa and C. Wilhelm, *ACS Nano*, 2019, **14**, 1406–1417.
73 Z. Wang, N. Sun, H. Liu, C. Chen, P. Ding, X. Yue, H. Zou, C. Xing and R. Pei, *ACS Appl. Mater. Interfaces*, 2019, **11**, 39586–39593.
74 T. Yoshino, H. Hirabe, M. Takahashi, M. Kuhara, H. Takeyama and T. Matsunaga, *Biotechnol. Bioeng.*, 2008, **101**, 470–477.
75 F. Mickoleit and D. Schüler, *Bioinspired, Biomimetic Nanobiomater.*, 2019, **8**, 86–98.
76 F. Mickoleit, C. Lanzloth and D. Schüler, *Small*, 2020, **16**, 1906922.
77 Z. Xiang, X. Yang, J. Xu, W. Lai, Z. Wang, Z. Hu, J. Tian, L. Geng and Q. Fang, *Biomaterials*, 2017, **115**, 53–64.
78 S. Schuerle, M. Furubayashi, A. P. Soleimany, T. Gwisai, W. Huang, C. Voigt and S. N. Bhatia, *ACS Synth. Biol.*, 2020, **9**, 392–401.
79 M. Boucher, F. Geffroy, S. Prévéral, L. Bellanger, E. Selingue, G. Adryanczyk-Perrier, M. Péan, C. T. Lefèvre, D. Pignol, N. Ginet and S. Mériaux, *Biomaterials*, 2017, **121**, 167–178.